Resolving Kinematic Redundancy in Teleoperated Laparoscopy: Force *vs* Torque Based Haptic Feedback

Joya Evans, Alec Cotton, and Carlos Rossa
Department of Systems and Computer Engineering
Carleton University, Ottawa, ON, Canada
joyaevans@cmail.carleton.ca; aleccotton@cmail.carleton.ca; carlos.rossa@carleton.ca

***Abstract*— Teleoperated laparoscopic systems often use articulated robotic tools controlled to pass through a remote centre of motion (RCM) at the entry point, restoring two degrees of freedom (DOF) lost during manual laparoscopy. When standard, non-articulated instruments are used, the RCM introduces kinematic redundancy between the human operator and the robot, as the console interface retains more DOF than the task requires. Existing approaches resolve this redundancy at the robot or task level, but do not explicitly address how it should be handled at the human interface. This paper treats redundancy as a user interaction problem and proposes two distinct strategies to enforce the RCM directly at the interface. In the first, the user is free to translate the device while its pitch and yaw are actively controlled to align with the tool axis. In the second, the user is free to orient the haptic device handle, and its position is regulated through force feedback to remain aligned with the RCM. Both methods are implemented and evaluated in a teleoperated simulation with three user groups performing identical tasks. The results show that both haptic strategies improve task efficiency and motion quality compared to no feedback. While overall performance is comparable between methods, the force-based approach better enforces alignment with the RCM, consistent with the higher force output capability of the device. These findings suggest that redundancy can be leveraged to enable different modes of user interaction with the environment, while maximizing the capabilities of the haptic interface without compromising intuitiveness or performance.**

I. Introduction

Laparoscopy is a minimally invasive surgical technique in which small incisions are made to insert long, slender instruments and a camera (laparoscope) into the abdominal cavity. The laparoscope provides real-time images of the internal anatomy, allowing the surgeon to perform procedures without large incisions. Compared to open surgery, laparoscopy inflicts less trauma and reduces recovery times and post-operative infection rates [1]–[5]. The advantages to the patient come at the expense of challenges for the surgeon: In open surgery, hand and wrist movement are unrestricted in 6 degrees of freedom (DOF). In laparoscopy, the incision point limits motion to 4 DOF: axial tool translation and rotation, and two rotational DOF (pitch and yaw) about a remote centre of motion (RCM) at the incision point [6], [7]. In addition, surgeons must contend with ergonomically taxing instrument positions, an unstable field of view, and reduced depth perception [8], [9].

While in traditional laparoscopy the surgeon operates directly on the patient, in robot-assisted laparoscopy they teleoperate robotic arms that manoeuvre the surgical tools from a separate console. This configuration can scale and filter the surgeon's motion and may provide 3D vision by fusing multiple camera images. Arguably, the major advantage of robot-assisted laparoscopy is the use of instruments with articulated tips, which restore the DOFs lost in conventional laparoscopy [10]. With 2-DOF articulated tool tips, the system enables the instruments to mimic the surgeon's hand and wrist movements in 6-DOF [11]. Robot-assisted laparoscopy is becoming the standard of care in urology, endocrinology, and general surgery in adult patients [12]–[14].

Robotic laparoscopy tools require large diameters (either 5 mm or 8 mm) to accommodate the articulated tip mechanism, and as a result, commercial systems such as the Da Vinci, Senhance, and Versius, are restricted exclusively to operating in the adult population. Paediatric patients, for example, have a smaller workspace and more fragile tissue structures compared to adults, making the use of articulated instruments impractical. A study showed that the Da Vinci system can successfully operate in patients below 15 kg and above 3 kg [15], but in neonates under 3 kg, traditional tools are inappropriate as they require a large workspace to function [16]. The standard in paediatric laparoscopy is the use of 3 mm in diameter tools, as they are more suitable for confined operations [17]. Although some researchers have proposed articulated paediatric tools, none are currently commercially available [18].

While restoring lost DOF with articulated instruments is beneficial, other advantages remain relevant even when using thin, unarticulated tools, including motion scaling, filtering, virtual fixtures [19], [20], and flexible port placement not limited by the surgeon's reach over the patient [8], [21]. When a robotic system with a 6-DOF console operates 4-DOF unarticulated tools, mapping the surgeon's motion to the tool tip becomes kinematically redundant; that is, there are more DOF available at the console than the robot can physically execute. An important question then arises: What are the best mapping strategies to resolve redundancy while optimizing intuitive operation? A mapping can be

We acknowledge the support of the Natural Sciences and Engineering Research Council of Canada (NSERC), [funding reference number RGPIN-2025-05468]. Cette recherche a été financée par le Conseil de recherches en sciences naturelles et en génie du Canada (CRSNG), [numéro de référence RGPIN-2025-05468].

implemented in which the console aligns its orientation with the teleoperated instrument, allowing the surgeon to feel as though they are holding the tool base while pivoting about a virtual RCM that mirrors a physical RCM at the robot level. Delta-type haptic interfaces commonly used in surgical consoles decouple translation and rotation and have vastly different force and torque capabilities. Motion mappings can also account for these asymmetries to ensure that the console remains aligned with the teleoperated tool while preserving intuitive operation.

In this paper, we compare two different motion mapping strategies between a 6-DOF haptic device and a virtual simulation of a laparoscopy task. Both mapping strategies are implemented to simulate an RCM at the console level through force or torque feedback, mimicking the RCM the operator sees in the simulation. These two methods are implemented as follows:

1) Method 1 - Torque feedback for orientation control: The user is free to translate the haptic device along the 3 Cartesian directions and rotate it about the longitudinal axis. To simulate an RCM, the device's pitch and yaw are enforced through torque feedback such that the console aligns itself with the tool passing through the RCM.

2) Method 2 - Force feedback for position control: Conversely, the user controls the device's pitch and yaw, and is free to translate it in the direction of tool insertion. The console's Cartesian position is enforced through force feedback such that it aligns itself with the RCM.

In both methods, the position of the device is mapped to the position of the tool tip in the simulation model, which enforces its own RCM. We compared these two methods using three user groups performing the same surgical task in a virtual environment. The first two groups used either Methods 1 or 2, respectively, while the third group received no force/torque feedback. User performance is evaluated based on completion time, path length, speed, acceleration, and jerk, while system performance is assessed on the alignment between the physical and virtual RCM. The results show that Methods 1 and 2 improve performance equally; however, Method 2 provides better alignment with the RCM axis, ensuring that the console is more closely aligned with the tool in the simulation.

Although prior work has simulated an RCM using virtual fixtures to restrict motion to admissible configurations [22], [23], and has addressed redundancy resolution in teleoperation [24], [25], these approaches formulate constraints at the task/robot level and do not explicitly resolve redundancy at the user interface. In contrast, this work treats redundancy as a haptic interaction problem and leverages it to enable the user to interact with the haptic device in two distinct ways: enforcing orientation through torques and enforcing position through forces. This perspective allows the same geometric constraint to be rendered through different channels, which can be adapted to specific force and torque anisotropy of the haptic device while maintaining task performance.

The remainder of this paper is structured as follows. Section II describes the simulated laparoscopy trainer designed and implemented for the purpose of this study, with a pair of 6-DOF haptic devices and a simulation model. Section III introduces the proposed motion mapping and force/torque feedback methods that simulate an RCM at the device level. The proposed methods are evaluated with user trials in Section IV, and the results and future work are discussed in Section V.

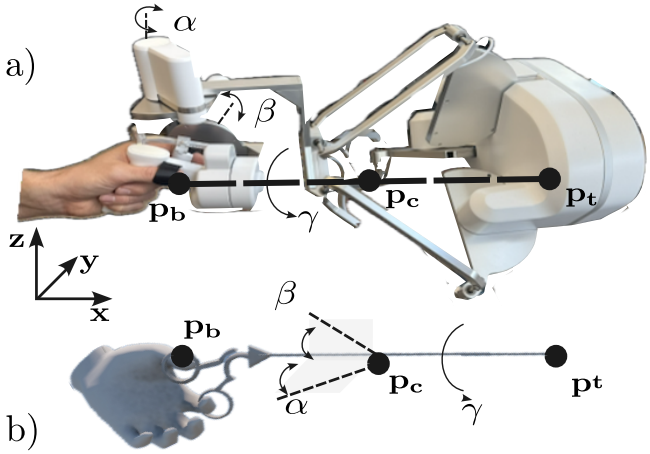


Fig. 1: The 6-DOF haptic device in a) teleoperates the laparoscopic tool in b), which passes through a remote centre of motion (RCM) at $\mathbf{p_c}$. The haptic device applies force or torques to the user's hand to orient itself in the direction of the teleoperated tool. The position of the tool base and tool tip are $\mathbf{p}_b$ and $\mathbf{p}_t$. The angles γ, β, α, represent the rotation of the tool about x, y, and z, respectively.

II. Simulated Laparoscopy Trainer with a Remote Centre of Motion

Consider the 6-DOF haptic device shown in Fig. 1(a). It controls the position and orientation of a teleoperated or virtual laparoscopic tool, as depicted in Fig. 1(b). The device is assumed to have a delta configuration, such that position and orientation are kinematically decoupled. In the simulation, the tool operates through an RCM, which we aim to reproduce at the haptic device level. To this end, the tool is assumed to be aligned with the last axis of the haptic device (i.e., along the user's arm). Force/torque feedback constrains the device's position or orientation such that the axis of the last joint always points toward the RCM. In this configuration, the tool roll angle γ about this axis is mapped directly to the tool roll in the simulation. As a result, 5 DOF remain at the haptic device, whereas only 3 DOF are required to fully define the tool pose when its shaft is constrained to pass through the virtual RCM.

Let $\mathbf{p}_b$ denote the 3-DOF position of the haptic device or tool base (bold variables denote column vectors, non-bold variables denote scalars). If the tool operates through an RCM located at $\mathbf{p}_c$, the tool tip position lies along the unit vector

$$\hat{\mathbf{u}} = \frac{\mathbf{p}_b - \mathbf{p}_c}{|\mathbf{p}_b - \mathbf{p}_c|} = [u_x \quad u_y \quad u_z]^T, \tag{1}$$

defined as pointing toward the tool base, where u_x, u_y, and u_z are the projections of $\hat{\mathbf{u}}$ onto the Cartesian axes x, y, and z, respectively, as defined in Fig. 1.

The tool tip position $\mathbf{p}_t$ is obtained by translating from $\mathbf{p}_b$ along $-\hat{\mathbf{u}}$ by the tool length ℓ_t:

$$\mathbf{p}_t = \mathbf{p}_b - \ell_t(\hat{\mathbf{u}}). \tag{2}$$

Conversely, given the device's pitch (rotation angle β about $\hat{\mathbf{y}}$) and yaw (rotation angle α about $\hat{\mathbf{z}}$), the unit vector $\hat{\mathbf{u}}$ can be reconstructed by defining the rotation matrices $\mathbf{R_z}(\alpha)$ and $\mathbf{R_y}(\beta)$, and a reference direction for $\hat{\mathbf{u}}$:

$$\hat{\mathbf{u}} = \mathbf{R_z}(\alpha)\mathbf{R_y}(\beta)(-\hat{\mathbf{x}}) = \begin{bmatrix} -\cos\alpha\cos\beta \\ -\cos\beta\sin\alpha \\ \sin\beta \end{bmatrix}. \tag{3}$$

The reference direction $\hat{\mathbf{x}} = [1 \quad 0 \quad 0]^T$ corresponds to $\hat{\mathbf{u}}$ aligned with $-\hat{\mathbf{x}}$, that is, when $(\alpha = 0)$ and $(\beta = 0)$. The yaw angle, or the azimuth of the projection of $\hat{\mathbf{u}}$ onto the xy plane is:

$$\alpha = \text{atan2}(-u_y, -u_x), \tag{4}$$

and the pitch is the projection of $\hat{\mathbf{u}}$ onto the xz plane:

$$\beta = \text{atan2}\left(u_z,\ \sqrt{u_x^2 + u_y^2}\right). \tag{5}$$

If pitch and yaw are considered the input to the haptic device, the required position of the tool base that makes segment $\overline{\mathbf{p}_b\mathbf{p}_c}$ collinear with $\hat{\mathbf{u}}$ is

$$\mathbf{p}_{b_d} = \mathbf{p}_c + (\ell_t - \ell_d)\hat{\mathbf{u}}, \tag{6}$$

where ℓ_d is the tool's insertion depth.

To control the haptic device through force or torque feedback such that the end effector mirrors the RCM, different strategies can be used. For example, the user is free to translate the haptic device in space, while the device actively adjusts pitch and yaw such that its last axis aligns with the tool. Alternatively, the delta configuration enables a strategy in which the user input is the haptic device's yaw and pitch, and the handle can only be translated along the direction of the tool (i.e., along $\hat{\mathbf{u}}$). The device then actively adjusts its position in space to align itself with the tool. Since delta haptic devices typically have higher force than torque capability, the second approach is expected to better enforce these constraints. However, this approach may be less intuitive and may affect performance, which has not been evaluated before. Other alternatives, involving partial control of both position and orientation, are theoretically possible at the expense of reduced intuitiveness and are therefore not considered in this work.

III. Constrained Motion

The two proposed methods apply force or torque feedback to align the haptic device in the direction of the RCM. The device's handle position is then transmitted to the simulation or teleoperation model, where a RCM constraint is enforced separately.

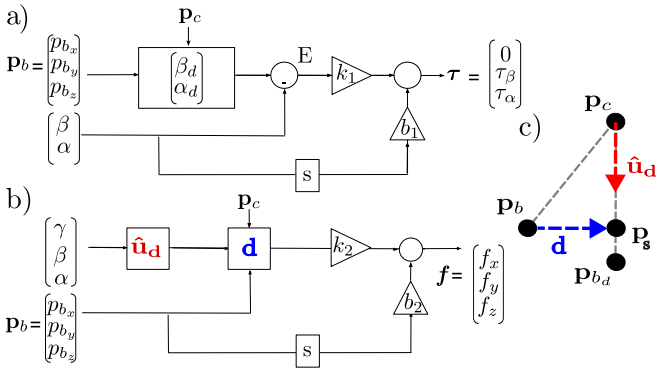


Fig. 2: a) Block diagram depicting how torque is generated in Method 1 from the measured handle position and current orientation, and how forces are generated in Method 2 from the measured handle orientation b). c) shows the correction displacement vector $\mathbf{d}$ that brings the handle to the axis of $\hat{\mathbf{u}}_d$ aligned with the RCM.

A. Method 1: Torque Feedback for Orientation Control

The first method allows the user to freely translate the haptic device's handle and rotate it about the last axis. The measured roll angle γ and the 3-DOF position of the handle are transmitted to the teleoperated site. Given the current position of the handle, let the resulting desired yaw and pitch angles calculated in (4) and (5) be α_d and β_d, respectively. To align the handle with the RCM, the haptic device applies torque τ_α about the z axis of the handle, given by the proportional-derivative controller:

$$\tau_\alpha = k_1(\alpha_d - \alpha) - b_1\frac{d\alpha}{dt}, \tag{7}$$

and applies torque τ_β about the y axis of the handle, defined in the same way as

$$\tau_\beta = k_1(\beta_d - \beta) - b_1\frac{d\beta}{dt}, \tag{8}$$

where k_1 and b_1 are tunable constants. The second term adds damping to prevent unwanted oscillations of the handle.

B. Method 2: Force feedback for Position Control

In the second method the user directly controls the pitch, yaw, and roll angles of the haptic device, which are measured and transmitted along with the tool insertion depth to the virtual or teleoperated site. Force feedback in the 3 Cartesian directions must be applied to align the haptic device's last joint in the direction of the RCM, while allowing the user to freely translate the handle along $\hat{\mathbf{u}}$.

In a haptic device with a delta kinematic configuration, rotation and translation are decoupled, therefore rotating the handle does not change the tool's insertion depth. Let $\mathbf{p}_{b_d}$ be the required position of the handle inferred from (3) that satisfies the RCM constraint for the user's input α and β. The forces that align the haptic device with the RCM can be obtained as:

$$\mathbf{f} = [f_x \quad f_y \quad f_z]^T = k_2(\mathbf{p}_{b_d} - \mathbf{p}_b) - b_2\frac{d\mathbf{p}_b}{dt} \tag{9}$$

where f_x, f_y, f_z are the forces along the x, y and z directions, and k_2 and b_2 are tunable parameters.

If handle rotation is not decoupled from translation (as in non-delta kinematic configurations), the handle must be moved while maintaining *nearly* the same distance from the RCM without force feedback along the direction of insertion. The formulation approximates this requirement for small displacements but guarantees free movement along the direction of insertion.

Referring to Fig. 1c), suppose that the user rotated and moved the handle from $\mathbf{p}_b$ to $\mathbf{p}_{b_d}$ given by (6). If $\hat{\mathbf{u}}_d$ is the desired orientation given by (3), we calculate the projection of segment $\overline{\mathbf{p}_b\mathbf{p}_c}$ onto $\hat{\mathbf{u}}_d$, that is, the point along $\hat{\mathbf{u}}_d$ with the shortest distance to $\mathbf{p}_b$ as:

$$\mathbf{p}_s = \mathbf{p}_c + [(\mathbf{p}_b - \mathbf{p}_c) \cdot \hat{\mathbf{u}}_d]\hat{\mathbf{u}}_d. \tag{10}$$

The correction vector that brings the haptic device to the axis of $\hat{\mathbf{u}}_d$ points from $\mathbf{p}_b$ to $\mathbf{p}_s$:

$$\mathbf{d} = \mathbf{p}_s - \mathbf{p}_b \tag{11}$$

which gives the force required to reposition the haptic device as:

$$\mathbf{f} = k_2\mathbf{d} - b_2\frac{d\mathbf{p}_b}{dt}, \tag{12}$$

Notice that $\mathbf{d}$ is perpendicular to $\mathbf{u}_d$, meaning that the force along $\mathbf{u}_d$ is zero (provided that $b_2 = 0$). For small displacements, this formulation maintains nearly constant distance from the RCM. To generalize Method 2 for both delta and non-delta kinematic configurations, force $\mathbf{f}$ is calculated using (12) in the experimental trials.

IV. Experimental Validation

To validate the proposed methods, we use the experimental setup shown in Fig. 3. It consists of two 6-DOF haptic devices (Lambda 7 from Force Dimension) with a gripper built in each handle. The user manipulates the haptic devices to control two laparoscopic tools in a virtual environment implemented in Unity. The position of the tool handle is measured and passed to the simulation, which determines the position of the tool tip as the shaft passes through the RCM in the simulation (see bottom of Fig. 3). Similarly, we implement a physical RCM at the device level, positioned at the centre of the workspace of the haptic device.

A peg transfer task is designed in the virtual environment to test dexterity through the user's ability to transfer rings between pegs. The model has 8 pegs, with 4 pegs on the left and right side respectively. The user must alternate passing the ring between the two tools when crossing from the right side to the left until the ring has been placed on each peg. The 12 sequential steps in the ring transfer sequence are outlined at the bottom of Fig. 3.

To evaluate the proposed force and torque feedback methods, 15 subjects consisting of students and staff from Carleton University with an average age of 25 years participated in the study. Five subjects were randomly assigned to each of 3 groups: **Group 1** completed the peg transfer task with Method 1 applied on the haptic devices. **Group 2** completed the peg transfer task using Method 2. **Group 3** did not have any torques or forces applied to the controller and thus motion was not limited by the RCM constraint. Pitch and yaw of the haptic device were neglected for Group 3. Following training with their assigned method, each subject completed 3 trials following the sequence shown in Fig. 3. Left and right haptic device position, orientation, and gripper opening are recorded at 200 Hz.

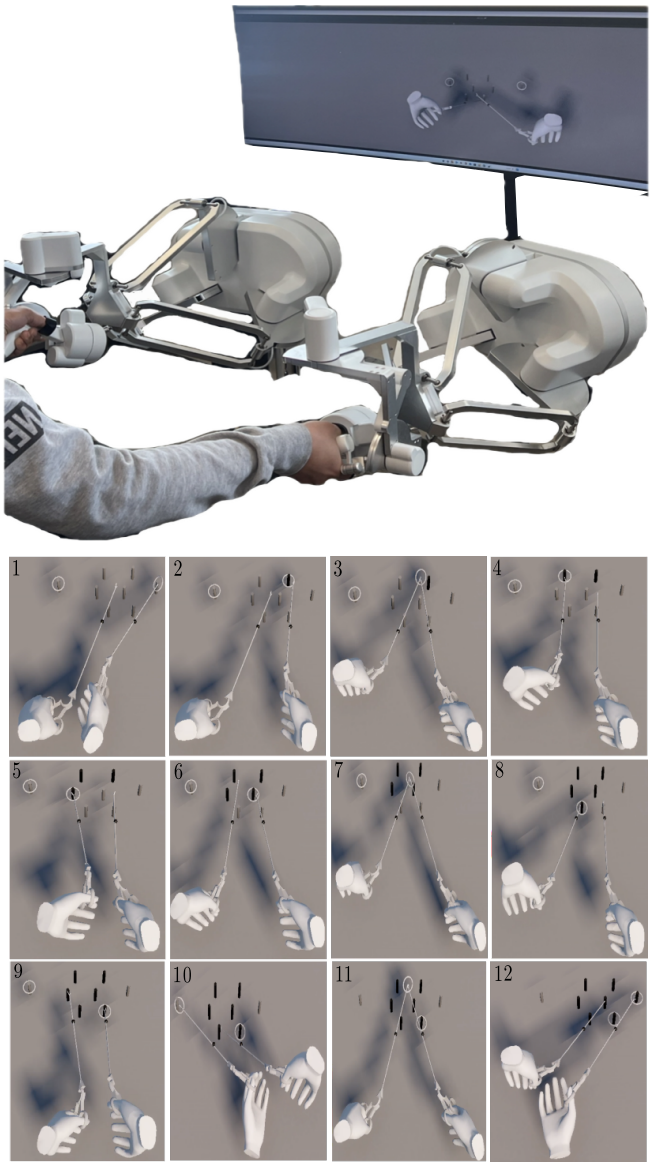


Fig. 3: Experimental setup with two 6-DOF haptic devices controlling the tool tip position $\mathbf{p}_t$ in the simulated virtual environment operating through a RCM. The bottom figure shows the 12 steps that constitute the peg transfer task sequence for the user trials.

Following the completion of a task, task efficiency is evaluated using completion time, path length, and the number of times the user opened or closed the gripper (hereafter, gripper events). Lower values indicate faster execution, more direct motion, and reduced unnecessary actuation of the gripper.

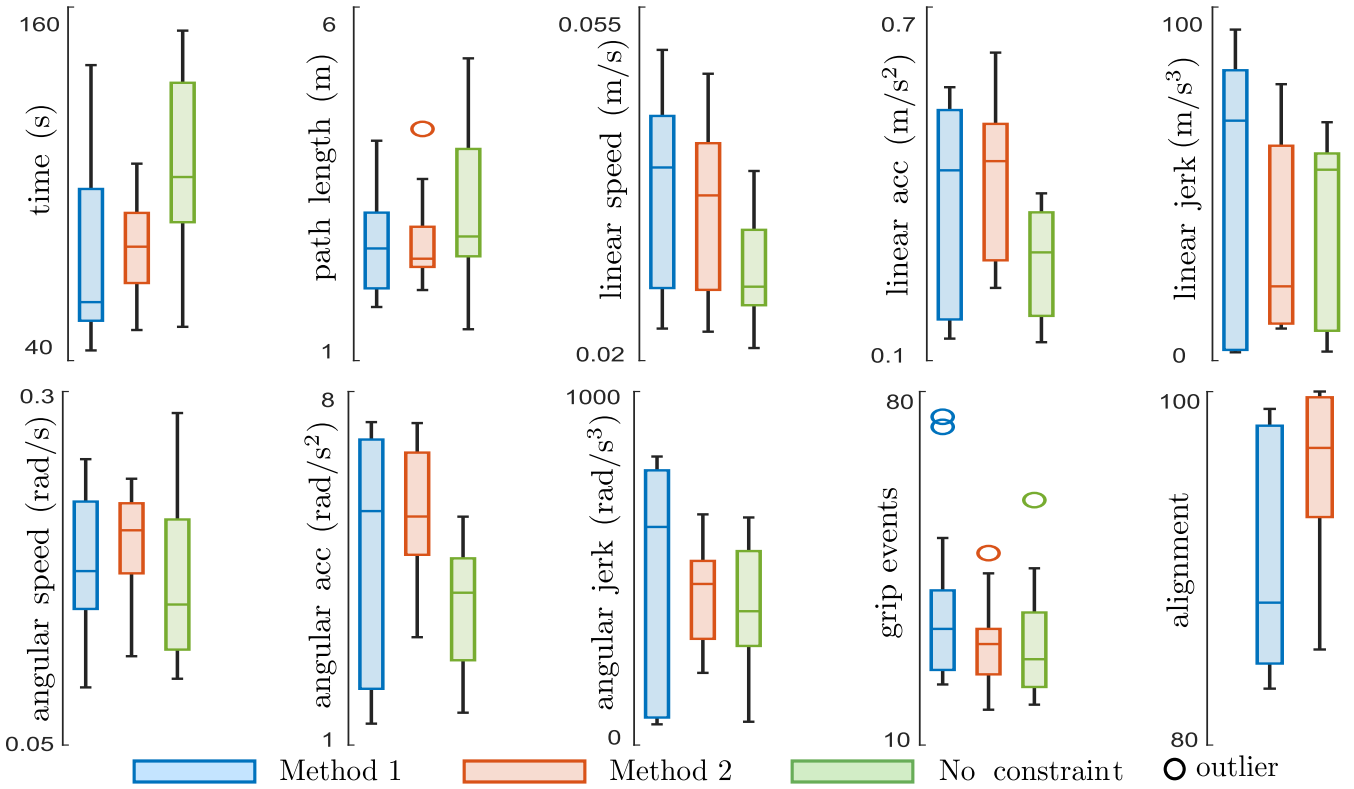


Fig. 4: Average and standard deviation of task performance metrics for each of the three user groups performing the peg transfer task using either Method 1, Method 2, or without force/torque feedback. Alignment is reported in percentage.

Motion stability and smoothness are quantified using the mean magnitude of linear and angular velocity, acceleration, and jerk. Alignment with the physical RCM is quantified by averaging the dot product between the current direction of the last joint of the haptic device $\hat{\mathbf{u}}$, and its desired direction $\hat{\mathbf{u}}_d$. This metric, reported as the average of $100(\hat{\mathbf{u}} \cdot \hat{\mathbf{u}}_d)$ over a trial, evaluates how the device enforces the RCM constraint, with values closer to 100 indicating better alignment.

The results are reported in Fig. 4. As expected, they show that introducing force or torque feedback to enforce a RCM constraint improves user performance across all evaluated metrics compared to no feedback. A one-way ANOVA indicated a significant effect on completion time ($F(2,12) = 4.15$, $p = 0.0405$, $\eta^2 = 0.389$). No significant differences were observed for the remaining performance metrics. Both Method 1 and Method 2 demonstrate a trend toward reducing completion time and a lower path length, indicating more efficient task execution and further suggesting that enforcing the RCM improves the user's perception of admissible motions, while reducing redundant or exploratory movements that usually arise during unconstrained manipulation.

In terms of motion analysis, linear and angular speed, acceleration, and jerk are lowest when no feedback is applied. This is expected because without actuation of the haptic device, the user is free to move it to any point and orientation in space. When force or torque feedback is applied, the device actively controls its position or orientation, partially explaining the increase observed in these metrics. Methods 1 and 2 show statistically similar performance, with Method 2 tending to consistently reduce angular and linear jerk. This suggests smoother and more stable motion, with fewer abrupt corrections when operating the device under Method 2. The reduction in jerk is particularly relevant, as it reflects improved motion continuity and reduced oscillations, which are often associated with poor motor control or uncertainty.

In terms of RCM enforcement, Method 2 achieves higher alignment with the RCM axis, indicating that enforcing position through forces is more effective than enforcing orientation through torques. This was an anticipated result, given that the haptic device used in the experiment has substantially higher force capability than torque capability. The slightly higher linear acceleration observed in Method 2 relative to Method 1 is consistent with this observation. This increase does not indicate worse control, but rather that the device applies stronger corrective forces. These results provide insight into an alternative way of rendering force or torque feedback, where the same geometric constraint can be enforced through different modalities tailored to the haptic device's capabilities, without compromising user performance.

V. Conclusion

This paper proposed two methods to resolve redundancy in teleoperated laparoscopic manipulation by enforcing an RCM constraint through kinaesthetic feedback. Such redundancy arises when a conventional surgical robot, designed to

operate with articulated surgical tools, operates with regular rigid instruments, resulting in the loss of 2 DOF at the operating site. As a result, there are more DOF at the console side than the robot can execute.

Two distinct motion mapping strategies are implemented and evaluated; one enforcing the constraint through orientation of the handle (via applied torques), and the second by enforcing the constraint through repositioning of the handle (via forces). The results from three distinct user groups show that both approaches improve task efficiency and motion quality compared to no force/torque feedback. This observation is consistent with the state of the art, confirming that force/torque feedback enhances intuitiveness and reduces unnecessary or inconsistent movements [24]. When comparing the two methods, the performance metrics are statistically similar, with Method 2 outperforming Method 1 in some of them. However, Method 2 shows better alignment with the RCM, as it uses a device with higher force than torque capability. This is reflected in the higher acceleration observed with Method 2, indicating stronger motion correction and active enforcement of the RCM. The results show a high standard deviation across all metrics. A more in-depth evaluation across different surgical tasks with a larger group of participants is required to further confirm these findings and generalize them across a wider number of surgical training scenarios.

While these results were captured over a small sample size, they suggest that the same geometric constraint can be rendered through different force and torque feedback modalities, offering more flexibility in how the user interacts with the system. The choice of motion mapping can be adapted to the force and torque capabilities of the haptic device without compromising user performance. Future work will focus on extending these methods to a physical system, where the virtual simulation model will be replaced with two surgical robots and evaluated with a larger number of users performing different surgical tasks.

VI. Ethics Statement

Carleton University's Research Ethics Board reviewed and approved the study involving human participants.

References

[1] A. Johnson, "Laparoscopic surgery," *The Lancet*, vol. 349, no. 9052, pp. 631–635, 1997.

[2] R. C. Frazee *et al.*, "A prospective randomized trial comparing open versus laparoscopic appendectomy.," *Ann Surg*, vol. 219, no. 6, pp. 725–731, 1994.

[3] F. Keus *et al.*, "Laparoscopic versus open cholecystectomy for patients with symptomatic cholecystolithiasis - Keus, F - 2006 | Cochrane Library," 2006.

[4] F. Coccolini *et al.*, "Open versus laparoscopic cholecystectomy in acute cholecystitis. Review and meta-analysis," *Int. J. of Surgery*, vol. 18, pp. 196–204, 2015.

[5] M. Tiwari *et al.*, "Safety, efficacy, and cost-effectiveness of common laparoscopic procedures," *Surg Endosc*, vol. 25, no. 4, pp. 1127–1135, 2011.

[6] Y. Tu *et al.*, "A review of wrist mechanism design and the application in gastrointestinal minimally invasive surgery of dof surgical laparoscopic instruments," *Surg Endosc*, vol. 39, no. 1, pp. 99–121, 2025.

[7] S. W. Wong and P. Crowe, "Visualisation ergonomics and robotic surgery," *J. Robot Surg*, vol. 17, no. 5, pp. 1873–1878, 2023.

[8] A. Supe, G. Kulkarni, and P. Supe, "Ergonomics in laparoscopic surgery," *J. of Minimal Access Surgery*, vol. 6, no. 2, pp. 31–36, 2010.

[9] G. Ballantyne, "The Pitfalls of Laparoscopic Surgery: Challenges for Robotics and Telerobotic Surgery," *Surgical Laparoscopy Endoscopy & Percutaneous Techniques*, vol. 12, no. 1, p. 1, 2002.

[10] L. T. Shen and J. Tou, "Application and prospects of robotic surgery in children: a scoping review," *World J. of Pediatric Surgery*, vol. 5, no. 4, 2022.

[11] K. Reddy *et al.*, "Advancements in Robotic Surgery: A Comprehensive Overview of Current Utilizations and Upcoming Frontiers," *Cureus*, 2023.

[12] K. Sheetz, J. Claflin, and J. Dimick, "Adoption of Robotic Surgery for Common Surgical Procedures," *JAMA Netw Open*, vol. 3, no. 1, p. 1918911, 2020.

[13] H. Koh *et al.*, "Efficacy and Safety of Robotic Procedures Performed Using the da Vinci Robotic Surgical System at a Single Institute in Korea: Experience with 10000 Cases," *Yonsei Med J*, vol. 59, no. 8, pp. 975–981, 2018.

[14] E. F. Smith and M. Okocha, "Robotic surgery in emergency general surgery: an overview of UK practice," *World J Emerg Surg*, vol. 20, p. 85, 2025.

[15] Q. Ballouhey *et al.*, "A comparison of robotic surgery in children weighing above and below 15.0 kg: size does not affect surgery success," *Surgical endoscopy*, vol. 29, no. 9, pp. 2643–2650, 2015.

[16] J. Meehan, "Robotic Surgery in Small Children: Is There Room for This?," *J. of Laparoend. & Advanced Surgical Techniques*, vol. 19, no. 5, pp. 707–712, 2009.

[17] T. Lobe *et al.*, "A SAGES technology and value assessment and pediatric committee evaluation of mini-laparoscopic instrumentation," *Surg Endosc*, vol. 36, no. 10, pp. 7077–7091, 2022.

[18] G. Wu *et al.*, "A 3 mm Wristed Instrument for the da Vinci Robot: Setup, Characterization, and Phantom Tests for Cleft Palate Repair," *IEEE Transactions on Medical Robotics and Bionics*, vol. 2, no. 2, pp. 130–139, 2020.

[19] A. Meinzer *et al.*, "Advances and Trends in Pediatric Minimally Invasive Surgery," *J. of Clinical Medicine*, vol. 9, no. 12, p. 3999, 2020.

[20] A. Spinelli *et al.*, "First experience in colorectal surgery with a new robotic platform with haptic feedback," *Colorectal Disease*, vol. 20, no. 3, pp. 228–235, 2018.

[21] G. van Haasteren, S. Levine, and W. Hayes, "Pediatric robotic surgery: early assessment," *Pediatrics*, vol. 124, no. 6, pp. 1642–1649, 2009.

[22] J. Luo, C. Yang, N. Wang, and M. Wang, "Enhanced teleoperation performance using hybrid control and virtual fixture," *Int. J. of Systems Science*, vol. 50, no. 3, pp. 451–462, 2019.

[23] V. Pruks and J.-H. Ryu, "Method for generating real-time interactive virtual fixture for shared teleoperation in unknown environments," *The Int. J. of Robotics Research*, vol. 41, no. 9-10, pp. 925–951, 2022.

[24] O. Wilz, B. Sainsbury, and C. Rossa, "Constrained haptic-guided shared control for collaborative human–robot percutaneous nephrolithotomy training," *Mechatronics*, vol. 75, p. 102528, 2021.

[25] A. Bini, V. Novelli, F. Porcini, A. Filippeschi, C. A. Avizzano, and A. Frisoli, "Null space exploration for enhanced transparency dissipation in tdpa-based teleoperation with redundant manipulators," in *2024 IEEE Conference on Telepresence*, pp. 5–9, IEEE, 2024.